Proceeding of the IEEE
International Conference on Robotics and Biomimetics
Dali, China, December 2019

A Piezoelectric Tactile Sensor and Human-inspired Tactile Exploration Strategy for Lump Palpation in Tele-operative Robotic Minimally Invasive Surgery

Feng Ju*, *Member, IEEE*, Yingxuan Zhang, Yahui Yun, Hao Guo, Xiaoyong Wei, Chengjun Zhu, Xianwang Zhang, Dongming Bai and Bai Chen

***Abstract*— A piezoelectric tactile sensor is proposed in this paper featuring small size suitable for minimally invasive surgery (MIS), simple structure with only one transducer for both actuation and sensing, and easy instrumentation requiring only electrical impedance measurement. Its validity and sensing performance are confirmed with simulations. In addition, the sensor together with a model of soft tissue with embedded lump are used to generate stiffness maps in various scenarios, which facilitate the construction of a virtual lump palpation system together with a vibrotactile feedback device and a visual tracking system. Subsequent experimental studies reveal that human palpation strategies have influence on the lump detection performance. The "Scanning" strategy leads to better performance in lump localization and size discrimination ratio, whereas the "Edge following" strategy achieves better performance in shape discrimination. Therefore, a combination of different palpation strategies is suggested which may help achieve the best performance in all aspects of the lump palpation task, and finally forms a human-inspired lump palpation solution that contributes to the robot-assisted MIS.**

I. Introduction

Manual palpation is routinely carried out by surgeons in open surgeries to identify lumps such as tumors which have higher stiffness than the surrounding soft tissues. However, this becomes difficult or even impossible in robot-assisted minimally invasive surgeries (MIS), since the surgeons are only allowed to tele-operate a remote console without haptic and tactile feedback [1]. The lost of touch sensation has been recognized as a major limitation of existing robotic MIS systems [2]. In order to solve this problem, research efforts are needed in areas of tactile sensor development, tactile exploration and tactile feedback. Although each of these areas have been investigated separately in the literature, there are still several technical issues remaining unsolved before a complete mature solution can be reached. For example, although tactile sensors of various principles have been proposed [3-8], a small one with diameter of a few millimeters, simple structure and instrumentation, and wide sensing range is always demanded. In the tactile exploration area, a few algorithms have been proposed based on techniques such as adaptive searching [9] and probabilistic techniques [10, 11]. However, a solution that stems from the nature of human palpation also deserves investigation and may leads to a new class of human-inspired palpation technique. Finally, a convergence work that combines all these three research aspects seems lacking in the literature that may help put all of them in a systematic framework to benefit from each other.

In this paper, we aim to carry out a preliminary convergence work to combine tactile sensor development, tactile feedback and tactile exploration. A piezoelectric tactile sensor is designed to generate stiffness maps in various scenarios of lump palpation, which facilitates the investigation of human palpation strategies together with a vibrotactile feedback device, for achieving a human-inspired lump palpation solution.

II. Tactile Sensor Design for Tissue Stiffness Sensing

A. Structure of the Tactile Sensor

A piezoelectric tactile sensor with diameter of 7 mm is developed for robotic palpation of lump in soft tissues. The structure of the sensor is shown in Fig. 1(a). It has three main components: a PZT (lead zirconate titanate) patch, a steel beam, and a steel tip. The PZT patch is attached on the upper surface of the steel beam. It acts as both the actuator and sensor with the unique technique called simultaneous actuation and sensing (SAS). The steel beam has two parts — a straight part and a spiral part. The straight part is where the PZT patch is attached. The spiral part is designed to reduce the resonant frequency of the sensor so that its operation frequency can be suitable for testing biological tissues. The steel cylinder with a hemispherical tip is for contacting with the tissue to test its stiffness (Fig. 1(b)).

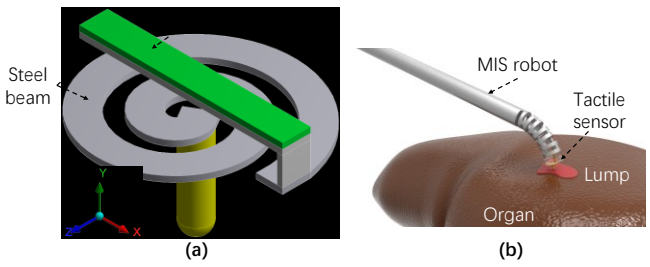

Figure 1. (a) Structure of the tactile sensor. (b) Potential application of the sensor in robot-assisted MIS.

* Corresponding author (Feng Ju). Feng Ju is with the College of Mechanical and Electrical Engineering, Nanjing University of Aeronautics and Astronautics, Nanjing, 210016 China. He is also with The State Key Laboratory of Fluid Power and Mechatronic Systems, Hangzhou, 310027 China (phone: +86-139-5189-2350; fax: 025-84891501; e-mail: juf@nuaa.edu.cn).

Yingxuan Zhang, Yahui Yun, Hao Guo, Xiaoyong Wei, Xianwang Zhang, Dongming Bai and Bai Chen are with the College of Mechanical and Electrical Engineering, Nanjing University of Aeronautics and Astronautics, Nanjing, 210016 China.

Chengjun Zhu is with the Department of Oncology, Jiangsu Province Hospital, Nanjing, 210029 China.

978-1-7281-6321-5/19//$31.00 ©2019 IEEE

B. *Stiffness Sensing Principle*

When an AC (alternating current) voltage is applied onto the electrodes of the PZT patch which is polarized in the Y-axis as illustrated in Fig. 2(a), cyclical expansion and contraction motion will be generated in the X-axis due to the inverse piezoelectric effect. As a result, the tip of the straight steel beam will be driven into vibration in the Y-axis. This vibration will further excite the spiral steel beam into vibration as well, and cause the cylindrical tip to dynamically interact with the test sample in contact with it. According to the equivalent circuit model in Fig. 2(b), electrical impedance Z_e of the PZT patch can be expressed by the following equation:

$$Z_e = \frac{\left(L_1C_1\omega^2 - 1\right) - j\left(R_1C_1\omega\right)}{\left(R_1C_0C_1\omega^2\right) + j\left[L_1C_0C_1\omega^3 - \omega\left(C_0 + C_1\right)\right]} \quad (1)$$

where C_0 is the electrical capacitance, R_1 is the mechanical dissipation, L_1 is the mechanical mass, C_1 is the mechanical compliance, and ω is the frequency. Example of Z_e is shown in Fig. 2(c). A local minimum in the curve indicates the resonance. The dynamic interaction between the sensor and the test sample will be coupled backward into the mechanical response of the sensor and finally electromechanically coupled into Z_e of the PZT patch due to the direct piezoelectric effect. Therefore, it is possible to detect the stiffness of the test sample from the Z_e. This will be further validated in the following simulation.

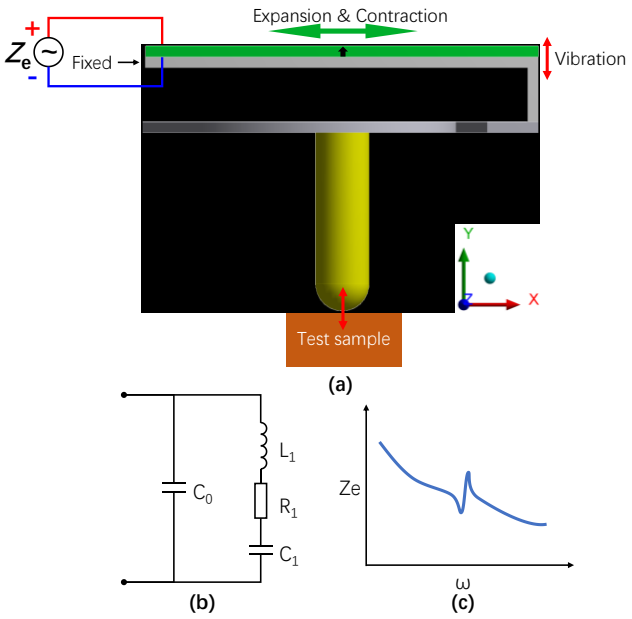

Figure 2. (a) Principle of stiffness sensing by simultaneous actuation and sensing capability of the sensor. (b) Equivalent circuit. (c) Electrical impedance curve.

C. *Simulation Study*

A finite element model is built for numerical simulation, as shown in Fig. 3(a). A spring with stiffness k is connected to the tip of the sensor as the load under test. The end of the steel beam and the other end of the spring are set into the fixed boundary conditions (B.C.). First, a harmonic response analysis is performed when the sensor is under free load ($k = 0$) to find its resonant frequency. A 0-1000 Hz swept sine voltage is applied to the sensor, and the electrical impedance curve is measured simultaneously. The free-load resonance is found at 698 Hz, which represents the first vibration mode of the sensor with the mode shape shown in Fig. 3(b). This validates that the designed sensor can be driven into vibration in the Y-axis for interacting with the test sample.

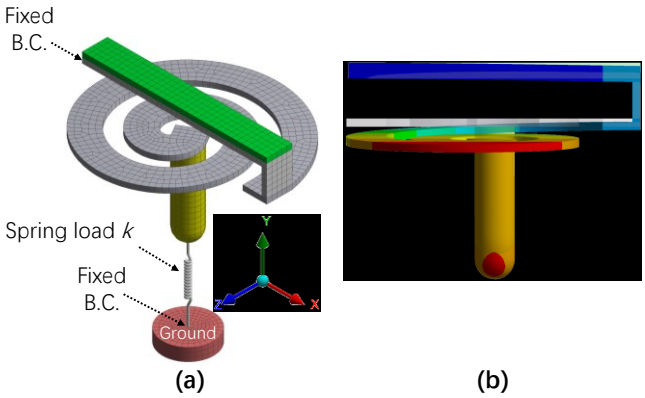

Figure 3. (a) FE model of the sensor. (b) Deformation of the sensor at its first vibration mode compared with the undeformed model (shadow).

After finding the resonant frequency, the operation frequency range of the sensor is narrowed down to 650-1000 Hz for the following simulations. A set of 9 different spring loads (k = 0, 50, 100, 200, 500, 1000, 2000, 5000 and 10000 N/m) in a wide stiffness range of 0-10000 N/m are tested by the sensor in harmonic response analyses. The electrical impedance curves are plotted in Fig. 4. It can be observed that the electrical impedance changes with the load under test. The valley in each curve indicates the resonance. The resonant frequency can be extracted as the feature of the electrical impedance curve to fit a model for calculating the stiffness of the load from measured electrical impedance.

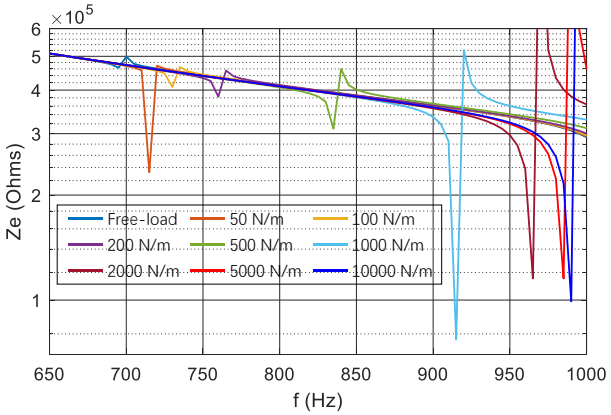

Figure 4. Electrical impedance curves measured in harmonic response analyses when loads of different stiffness values are tested.

The resonant frequencies under different test loads are extracted and plotted in Fig. 5 against the stiffness. It shows that the sensitivity of the sensor is high when k is less than 2000 N/m. It becomes less sensitive in the range of 2000-5000 N/m and almost insensitive in the range of 5000-10000 N/m. Therefore, the designed sensor is most effective in the 0-2000 N/m stiffness range, which is sufficiently wide for representing biological tissues from very soft to very hard (Young's modulus 0-2 MPa) [7]. An exponential model is

fitted with the 9 test points and plotted in Fig. 5. A good fitting performance is achieved with R^2 of 0.996. No over-fitting is found since the curve is smooth and no fluctuation is observed between adjacent data points. This analytical model can be used to calculate the stiffness of an unknown load from the tested electrical impedance.

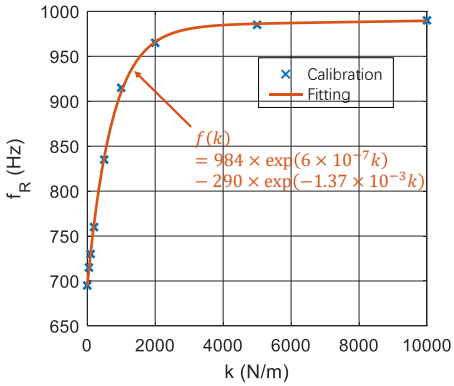

Figure 5. Resonant frequencies extracted from the electrical impedance curves and a fitted analytical model.

III. Investigation of Human Palpation Strategy for Lump Exploration

The strategy of robotic tactile exploration for lump localization and identification can be inspired by human behavior. When a person is asked to palpate an unknown soft object to find the location and shape of an embedded lump, he/she may use strategies such as scanning, random sampling, and edge following. It is hypothesized that some of the strategies may help him/her achieve the highest efficiency and accuracy. This hypothesis will be tested in the following experiment with the stiffness maps acquired with the FE model, and a vibrotactile feedback device for displaying the stiffness value to the user's fingertip.

A. Lump Palpation System Configuration

A FE model of a soft tissue is built for generating the stiffness map used in the palpation experiment, as shown in Fig. 6. An unknown lump is embedded into the soft tissue. Three shapes and three sizes of the lump are simulated as illustrated in Fig. 6(a-c) and listed in Tab. I. The combination of shape and size results in 9 simulation cases labelled as "CS, CM, CL, SS, SM, SL, TS, TM, TL", where the first letter stands for the shape (C — circular, S — square, T — triangular), and the second letter stands for the size (S — small, M — medium, L — large). The tissue model is then palpated by the tactile sensor to form a stiffness map, as illustrated in Fig. 7. The color in the stiffness map represents the stiffness value with red being the lowest (soft) and blue being the highest (hard). It can be observed that the stiffness map is not binary-valued with some points having values between "soft" and "hard" due to the edge and corner effect. This will be considered during the mapping from stiffness to vibrotactile feedback.

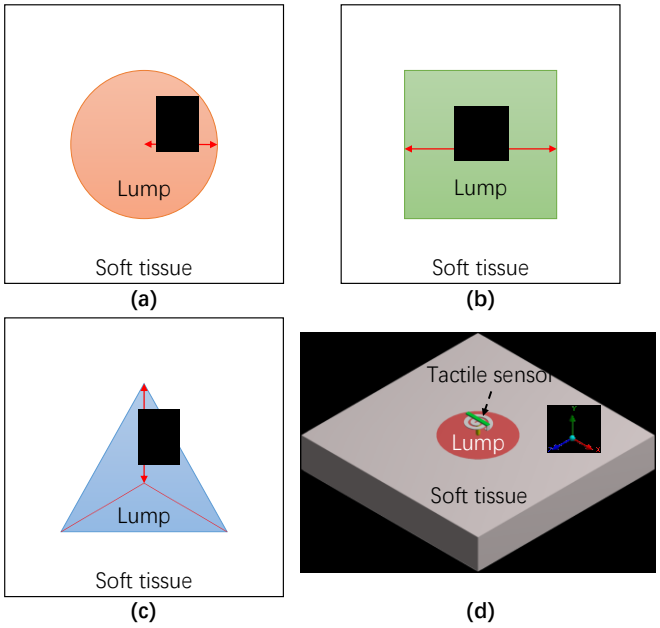

Figure 6. FE simulation with different lump shapes. (a) Circular. (b) Square. (c) Triangular. (d) FE model.

TABLE I. Different Lump Sizes in the Simulation and Experiment

Case No.	Shape	Lump Size	
		Label	*r (mm)*
1	Circular	CS	10
2		CM	20
3		CL	30
4	Square	SS	10
5		SM	20
6		SL	30
7	Triangular	TS	10
8		TM	20
9		TL	30

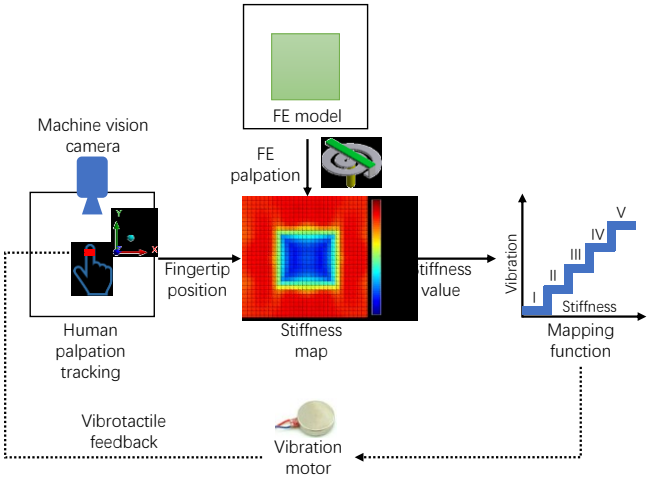

Figure 7. Lump palpation system configuration diagram.

A machine vision camera is used to track the position of the participant's fingertip. The fingertip position is then input to the stiffness map to find the stiffness value at that position.

A vibration motor is used to display the stiffness value to the user's fingertip. It generates vibration when voltage is applied. The intensity of vibration stimulus can be controlled by the amplitude of the excitation voltage. A staircase function shown in Fig. 7 is used as the mapping function to convert the stiffness value into 5 vibration levels (I, II, III, IV, and V). According to our previous experimental study on human hand's sensitivity to vibration stimulus [12], the 5 driving voltages in Tab. II are used to generate vibration stimuli which are the most discriminable by human hand. The driving voltage is achieved in our experiment by pulse width modulation (PWM) with the duty cycle also listed in Tab. II.

TABLE II. HUMAN HAND'S MOST DISCRIMINABLE VIBRATION STIMULI GENERATED BY A VIBRATION MOTOR

Vibration Level	Driving Voltage (V)	PWM Duty Cycle
I	1	20%
II	1.5	30%
III	2	40%
IV	3	60%
V	4	80%

B. Experiment Setup

A machine vision tracking and vibrotactile feedback system for lump palpation is implemented in Fig. 8(a). A Basler ace acA1300-200uc machine vision camera is used to track the fingertip position based on the Mean Shift visual tracking algorithm implemented in LabVIEW. The fingertip is marked with a small piece of red tape, as shown in Fig. 8(b). The stiffness map, the lookup table algorithm, and the mapping algorithm are also implemented in LabVIEW. NI USB-7865R Multifunction Reconfigurable DAQ from National Instruments (Austin, TX) is used to generate the PWM for driving the vibration motor which is attached to the participant's fingertip with a transparent finger cot. The trajectory of the fingertip during the test is recorded as shown in Fig. 8(c).

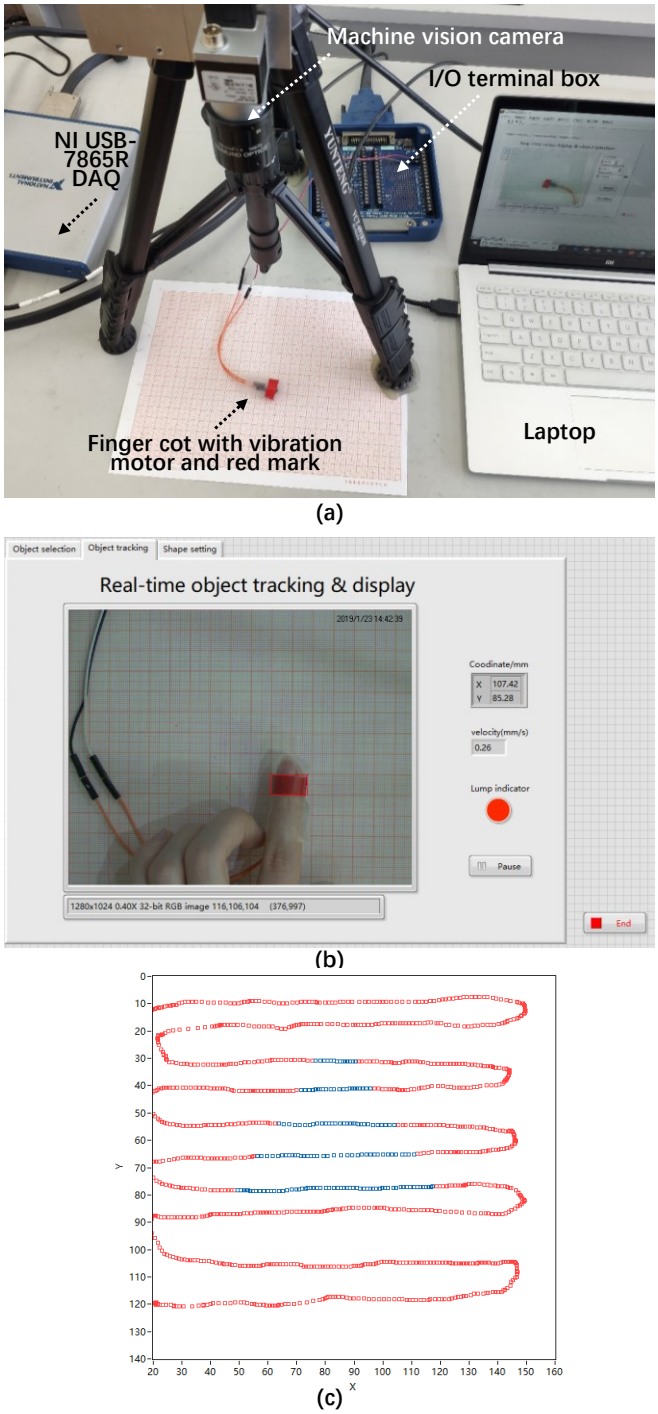

Figure 8. Experiment setup for lump palpation with human fingertip. (a) Hardware setup. (b) Software GUI. (c) Example of the fingertip trajectory (red color indicates the sampled points in the trajectory outside the shape to detect, blue color indicates the sampled points inside the shape to detect).

C. Lump Localization

A lump detection and localization experiment is first conducted on 22 subjects (11 female and 11 male) aged between 21 and 32 years. The participants are informed of all the procedures and familiarized with the hardware and software before the test. After putting on the finger cot and initializing the visual tracking program, the participant is asked to move his/her finger with a constant velocity (30 mm/s)

to find a randomly located circular lump (CM) and estimate its center location within 30 seconds. The participant is allowed to freely use any strategies he/she likes. The estimated lump location as well as the time to make decision are recorded and analyzed to calculate the mean and standard deviation (S.D.). This data set is labelled as "Free".

A discussion with the participants after the first test reveals that some participants have used strategies such as scanning and edge following. In order to find whether these strategies can help improving palpation performance, a second test is carried out in which the participant is asked to detect and localize the same lump (CM) with the scanning strategy. This data set is labelled as "Scanning". A third test is then carried out by limiting the participants to use the edge following strategy. The data set is labelled as "Edge following".

The results are presented in Fig. 9 as bar plots. Fig. 9(a) is the distance from the detected lump location to the actual location. It shows that the "Free" case has the largest distance as well as variance in the estimation, whereas the "Scanning" case has the smallest. The time to make decision in Fig. 9(b) shows that the "Edge following" strategy leads to a shortest decision time, whereas the "Scanning" strategy results in the longest. These results indicate that the "Scanning" strategy has the highest accuracy in detecting the location of an unknown lump, whereas the "Edge following" strategy has the highest efficiency.

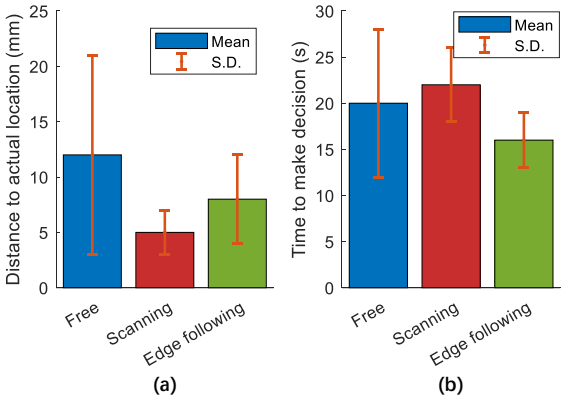

Figure 9. Results of the lump localization experiment. (a) Distance from the detected lump location to the actual location. (b) Time to make decision.

D. Lump Shape and Size Discrimination

A lump shape discrimination experiment is then conducted in which the participants are asked to identify the shape of an unknown lump, which is randomly selected from "CM", "SM" and "TM". Similar to the previous experiment, 3 tests are carried out with the 3 palpation strategies — "Free", "Scanning" and "Edge following", respectively. In each test, the participant needs to palpate the object within 30 seconds and estimate the shape of it. He/she will score 1 point if the estimation is correct, and otherwise 0 point. Each test is repeated 10 times for each participant. The scores in each of the three tests are then summed up to calculate the discrimination ratio which is plotted in Fig. 10(a). It shows that the "Edge following" strategy has the highest discrimination ratio compared to the other two, whereas the "Free" case has the lowest. This confirms the effect of palpation strategy on the discrimination performance.

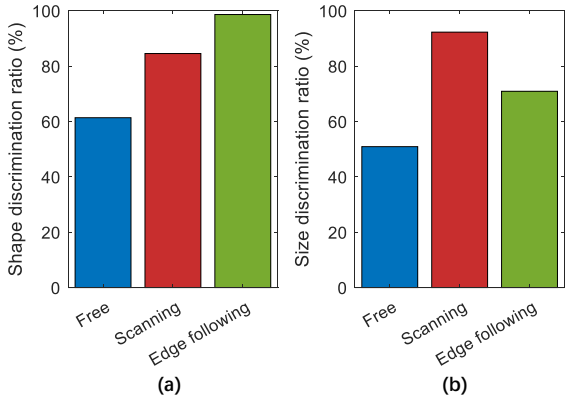

Figure 10. Results of the lump discrimination experiments. (a) Shape discrimination. (b) Size discrimination.

Finally, a lump size discrimination experiment is conducted in which the participants are asked to detect an unknown lump and estimate its size (S, M, or L) as defined in Fig. 6 and Tab. I. All the test cases in Tab. II are randomly presented and the participant is asked to estimate the size with the three palpation strategies, respectively. He/she will score 1 point if the identified size matches with the actual size, and otherwise 0 point. The scores in each of the three tests are then summed up to calculate the discrimination ratio which is plotted in Fig. 10(b). It shows that the "Scanning" strategy has the highest discrimination ratio, whereas the "Free" case has the lowest.

IV. Conclusion

A piezoelectric tactile sensor is designed for tissue stiffness detection in robot-assisted MIS procedures. Its validity and sensing performance are confirmed with FE simulations. The sensor as well as the FE model of a soft tissue with an embedded lump are then used to generate stiffness maps for constructing a virtual lump palpation system for investigating the influence of human palpation strategies on the performance of lump detection.

The palpation experiments clearly show that palpation strategies do have influence on the lump detection performance. It is also observed that different strategies have different effects on the detection result. The "Scanning" strategy can increase the localization accuracy as well as the size discrimination ratio. However, it will increase the detection time and lead to non-optimal shape discrimination performance. On the contrary, the "Edge following" strategy can achieve better performance in shape discrimination. But its performance in localization and size discrimination is lower, although still much higher than that in the "Free" case. Therefore, a combination of different palpation strategies may help achieve the best performance in all aspects of the lump palpation task. This will be investigated in future studies.

V. ACKNOWLEDGEMENTS

This work is supported by National Natural Science Foundation of China (No. 61973335), Natural Science Foundation of Jiangsu Province under Grant BK20191272, “the Fundamental Research Funds for the Central Universities, NO. NS2018033”, and also funded by Open Foundation of the State Key Laboratory of Fluid Power and Mechatronic Systems (GZKF-201711).

REFERENCES

[1] S. C. Lim, H. K. Lee, and J. Park, "Role of combined tactile and kinesthetic feedback in minimally invasive surgery," *International Journal of Medical Robotics and Computer Assisted Surgery*, vol. 11, pp. 360-374, Sep 2015.

[2] N. Simaan, R. M. Yasin, and L. Wang, "Medical Technologies and Challenges of Robot-Assisted Minimally Invasive Intervention and Diagnostics," *Annual Review of Control, Robotics, and Autonomous Systems*, vol. 1, pp. 465-490, 2018.

[3] L. Zou, C. Ge, Z. J. Wang, E. Cretu, and X. O. Li, "Novel Tactile Sensor Technology and Smart Tactile Sensing Systems: A Review," *Sensors*, vol. 17, p. 24, Nov 2017.

[4] X. L. Chen, J. Y. Shao, H. M. Tian, X. M. Li, Y. Z. Tian, and C. Wang, "Flexible three-axial tactile sensors with microstructure-enhanced piezoelectric effect and specially-arranged piezoelectric arrays," *Smart Materials and Structures*, vol. 27, p. 11, Feb 2018.

[5] F. Ju and S. F. Ling, "Bioinspired active whisker sensor for robotic vibrissal tactile sensing," *Smart Materials and Structures*, vol. 23, p. 9, Dec 2014.

[6] A. S. Naidu, M. D. Naish, and R. V. Patel, "A Breakthrough in Tumor Localization Combining Tactile Sensing and Ultrasound to Improve Tumor Localization in Robotics-Assisted Minimally Invasive Surgery," *Ieee Robotics & Automation Magazine*, vol. 24, pp. 54-62, Jun 2017.

[7] L. Zhang, F. Ju, Y. F. Cao, Y. Y. Wang, and B. Chen, "A tactile sensor for measuring hardness of soft tissue with applications to minimally invasive surgery," *Sensors and Actuators a-Physical*, vol. 266, pp. 197-204, Oct 2017.

[8] S. McKinley, A. Garg, S. Sen, R. Kapadia, A. Murali, K. Nichols, et al., "A Single-Use Haptic Palpation Probe for Locating Subcutaneous Blood Vessels in Robot-Assisted Minimally Invasive Surgery," in *2015 International Conference on Automation Science and Engineering*, ed New York: Ieee, 2015, pp. 1151-1158.

[9] R. E. Goldman, A. Bajo, and N. Simaan, “Algorithms for autonomous exploration and estimation in compliant environments”. *Robotica*, 2013, 31(1): 71-87.

[10] K. A. Nichols, and A. M. Okamura, "Autonomous robotic palpation: Machine learning techniques to identify hard inclusions in soft tissues." *2013 IEEE International Conference on Robotics and Automation (ICRA)*. IEEE, 2013.

[11] H. Salman, et al. "Trajectory-optimized sensing for active search of tissue abnormalities in robotic surgery." *2018 IEEE International Conference on Robotics and Automation (ICRA)*. IEEE, 2018.

[12] D. Bai, F. Ju, F. Qi, et al. “A wearable vibrotactile system for distributed guidance in teleoperation and virtual environments”. *Proceedings of the Institution of Mechanical Engineers, Part H: Journal of Engineering in Medicine*, 2018: 0954411918821387.